Supporting information - Figures

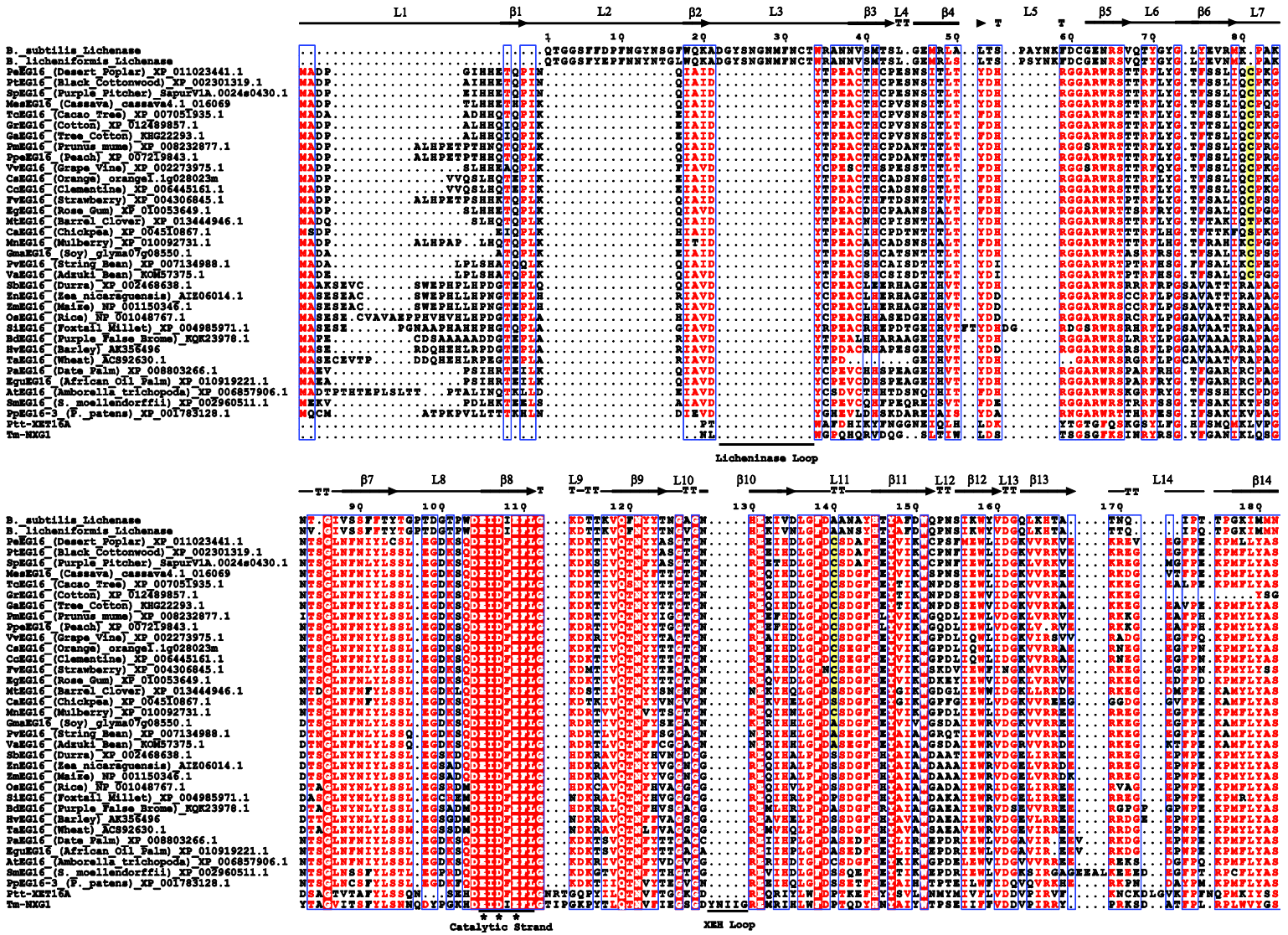

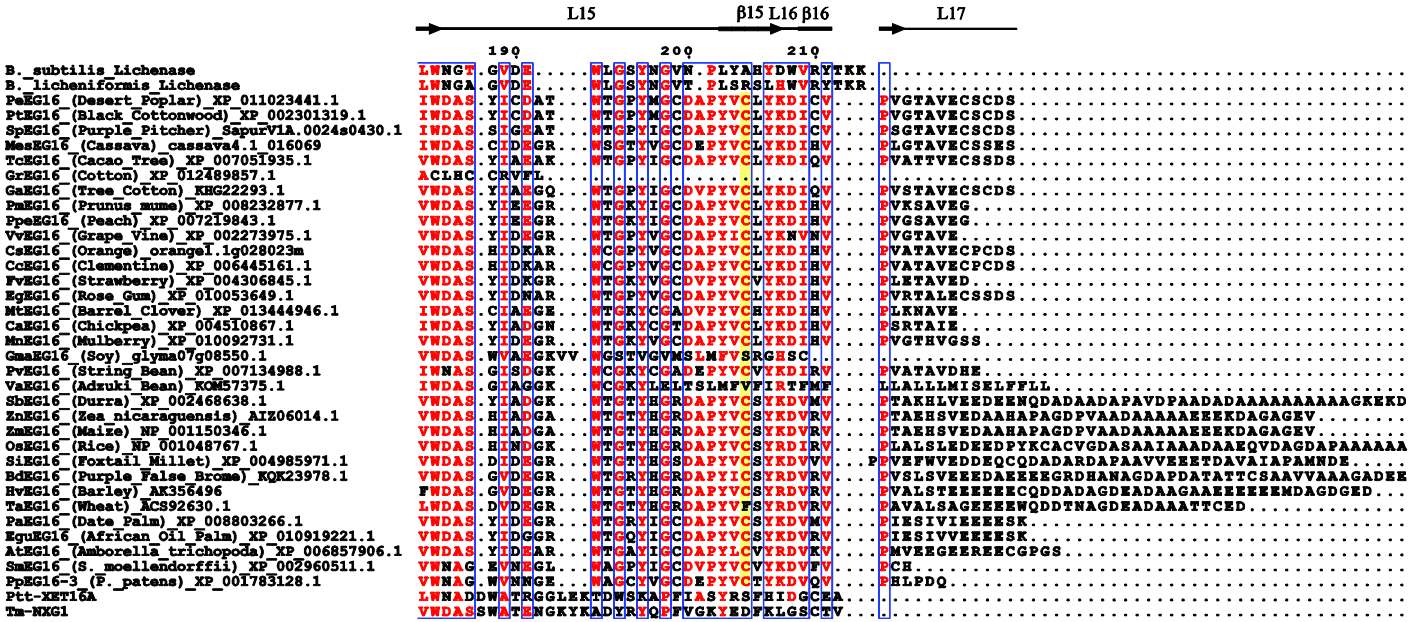

Figure S1: Protein sequence alignment of EG16s with Licheninases and *XTH* gene products. EG16s are named according to the first letters of their genus and species names. For each EG16, the common name (where available) for the plant of origin is given along with the accession code for the gene product. Regions of high similarity are shown in red. Secondary structure features, defined based on the crystal structure of VvEG16(ΔV152,E89A) in complex with cellooligosaccharides, are displayed and named above the alignment. Conserved cysteines among monocot or dicot EG16s are highlighted in yellow. The licheninases loop, XEH loop and catalytic strand are labelled below the sequences, stars mark the catalytic nucleophile, general acid/base and "helper" aspartic acid.

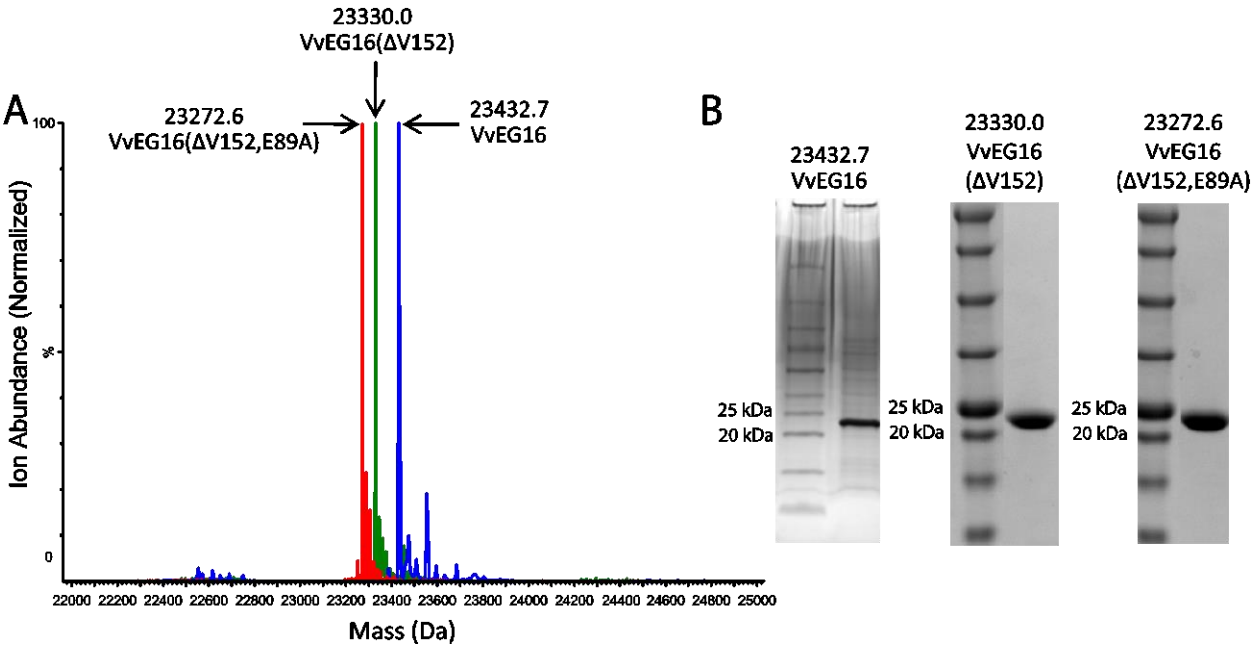

Figure S2: Analysis of purified VvEG16 proteins. A) Reconstructed intact mass spectra of VvEG16, VvEG16(ΔV152) and VvEG16(ΔV152,E89A). The purified proteins had masses of 23432.7 (expected 23432.1), 23330.0 Da (expected 23331.0), and 23272.6 Da (expected 23272.9) respectively, verifying that the protein sequence was correct, demonstrating that no post-translational modifications were present after TEV protease cleavage of the His_6 affinity tag and suggesting that all cysteine residues were reduced. B) SDS-PAGE analysis of purified VvEG16, VvEG16(ΔV152) and VvEG16 (ΔV152,E89A) after TEV protease cleavage.

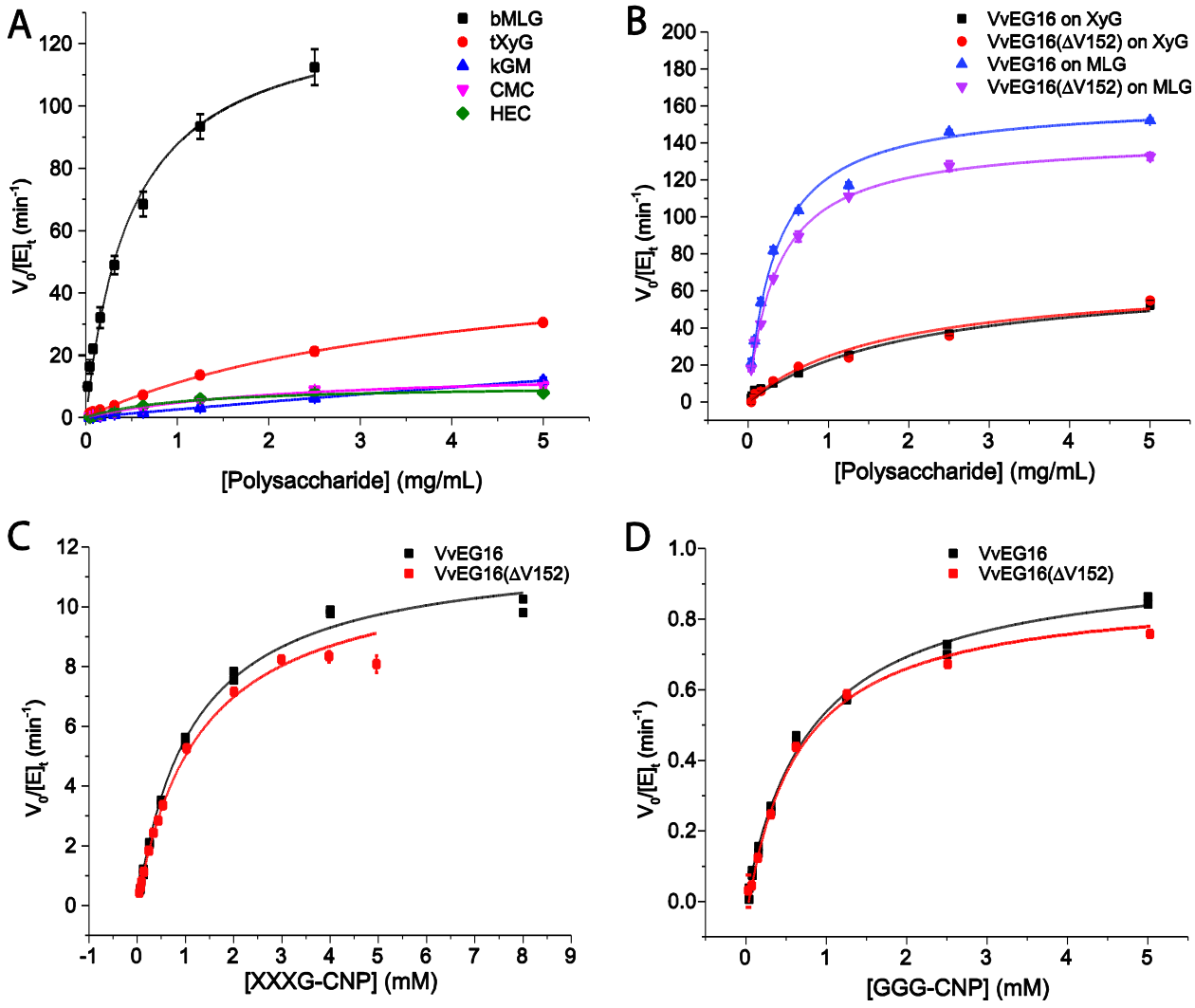

Figure S3: Comparison of wild-type VvEG16 and VvEG16 (ΔV152) activities. A) Overlay of wild-type VvEG16 and VvEG16 (ΔV152) acting bMLG and tXyG. B) Kinetics of VvEG16(ΔV152) acting on various polysaccharide substrates. C) Comparison of wild-type VvEG16 and VvEG16(ΔV152) acting XXXG-CNP. D) Comparison of wild-type VvEG16 and VvEG16(ΔV152) acting GGG-CNP. Each data point represents the average of two replicates. Activity of VvEG16(ΔV152) on a variety of polysaccharides at a variety of concentrations. Kinetics were modelled to extract apparent k_{cat} and K_M values based on the Michaelis-Menten curves shown. Error bars represent the standard deviation of three technical replicates.

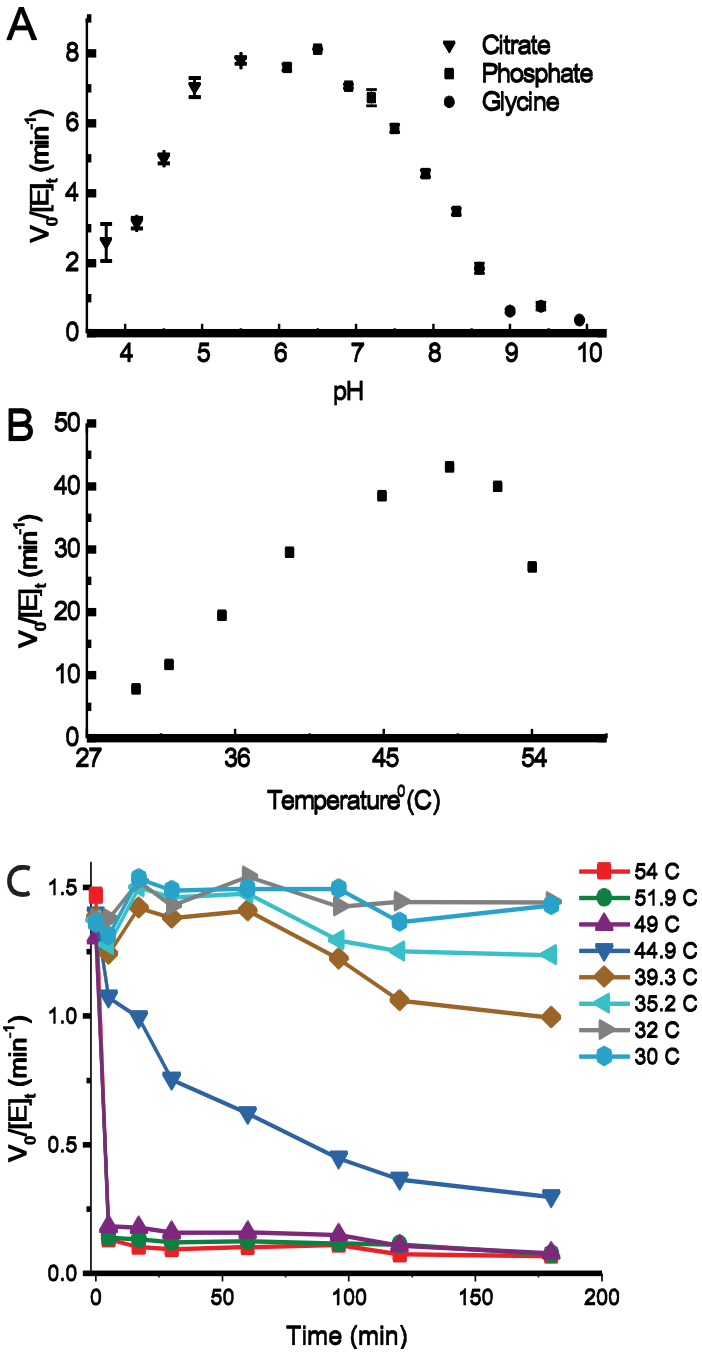

Figure S4: Dependence of VvEG16(ΔV152) activity on pH and temperature. A) Activity of VvEG16(ΔV152) on 1 mg/mL tXyG in buffers at various pH values measured using the BCA assay. Error bars represent that standard deviation of three technical replicates. B) Activity of VvEG16(ΔV152) on 1 mg/mL tXyG in pH 6.0 sodium citrate buffer at various temperatures measured using the BCA assay. Each data point represents the average of two technical replicates. Reactions were incubated for 15 minutes with no reducing agent present prior to quenching by the addition of BCA reagent. C) Thermal stability of VvEG16(ΔV152) in dithiothreitol-containing buffer. Activity on 1 mM XXXG-CNP was measured at room temperature at regular intervals during incubation of the enzyme at various temperatures in pH 5.5 sodium citrate.

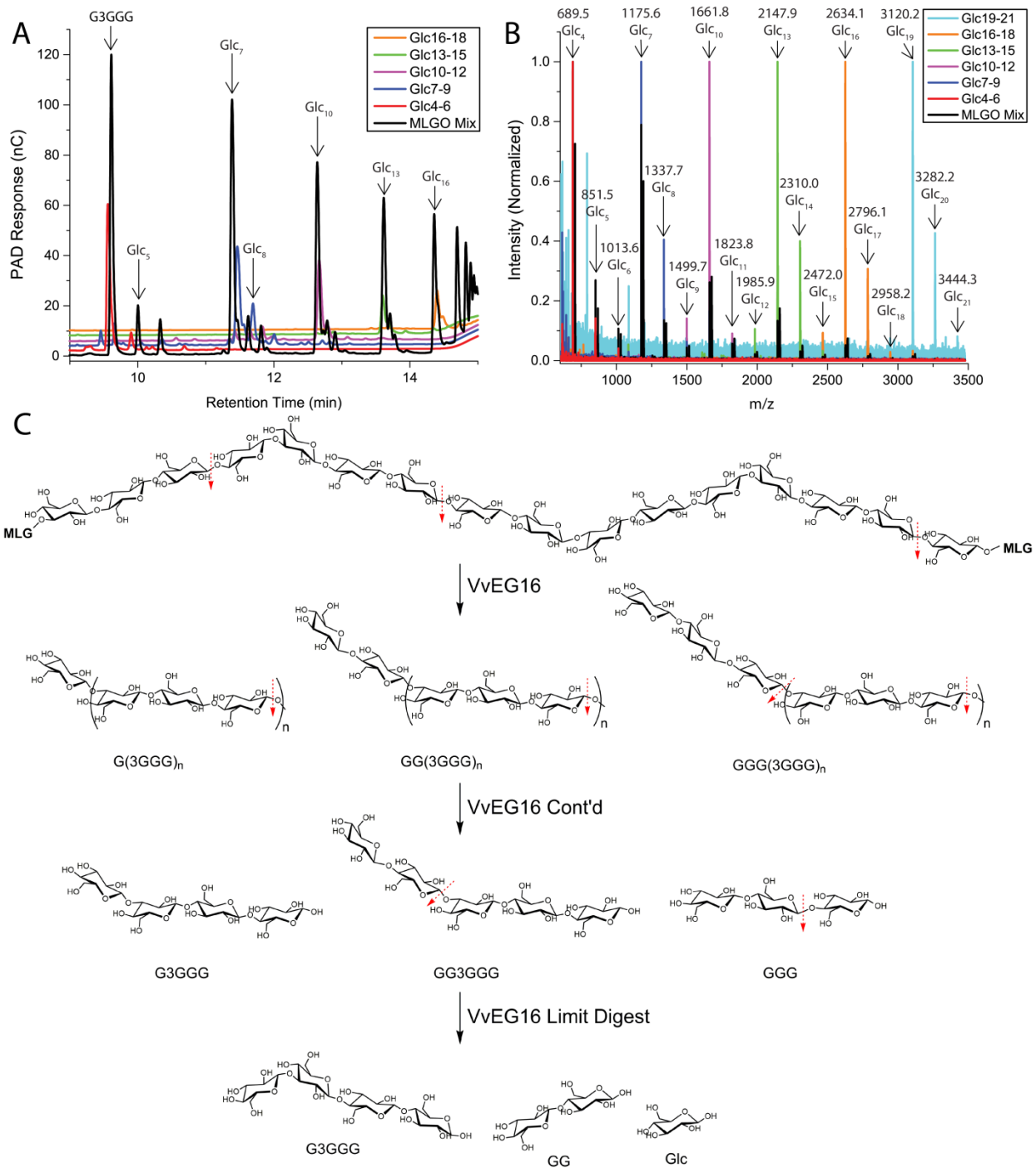

Figure S5: Identification of oligosaccharide series produced by action of VvEG16(ΔV152) on bMLG. Oligosaccharides were separated by size using a SEC column and analyzed by HPAEC-PAD (panel A) and MALDI-TOF (panel B) to determine the mass corresponding to each HPAEC-PAD peak. Panel C depicts a schematic of bMLG breakdown by VvEG16. bMLG polysaccharide (top) is initially cleaved by VvEG16 at β1,4 bonds following cellotriose motifs. The resulting oligosaccharides (second from top) contain repeating β1,3-linked cellotriose motifs terminated at the non-reducing end with primarily β1,3-linked glucose (~90%) and less commonly β1,3-linked cellobiose (~5%) or cellotriose motifs (~3%). This

gives rise to the three nested series of peaks observed in panel A. Continued digestion of these oligosaccharides gives the three oligosaccharides shown (second from bottom). Finally, slow hydrolysis of the pentasaccharide and cellotriose give the final products observed in the limit digest (figure 2C,D): glucose, cellobiose and G3GGG which cannot be further broken down by VvEG16.

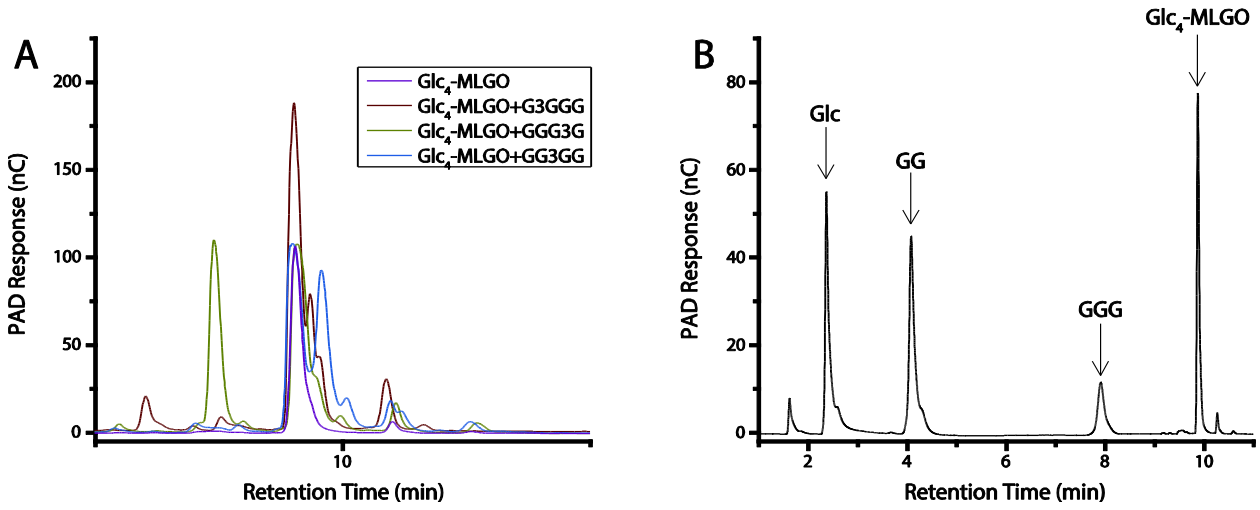

Figure S6: Identification of the MLGO produced by the action of VvEG16(ΔV152) on bMLG (Glc_4-MLGO) by HPAEC-PAD. A) 10 µM Glc_4-MLGO was mixed 1:1 with water or 10 µM standards of G3GGG, GG3GG and GGG3G and run with gradient B. Notably, the Glc_4-MLGO peak co-eluted with G3GGG and grew when G3GGG was added. B) Further confirmation of the identity of Glc_4-MLGO was obtained by partial digestion with an exo-acting β-glucosidase. Only G, GG and GGG were observed as products, thus confirming that the β(1,3) linkage was found between the two non-reducing-terminal glucose residues.

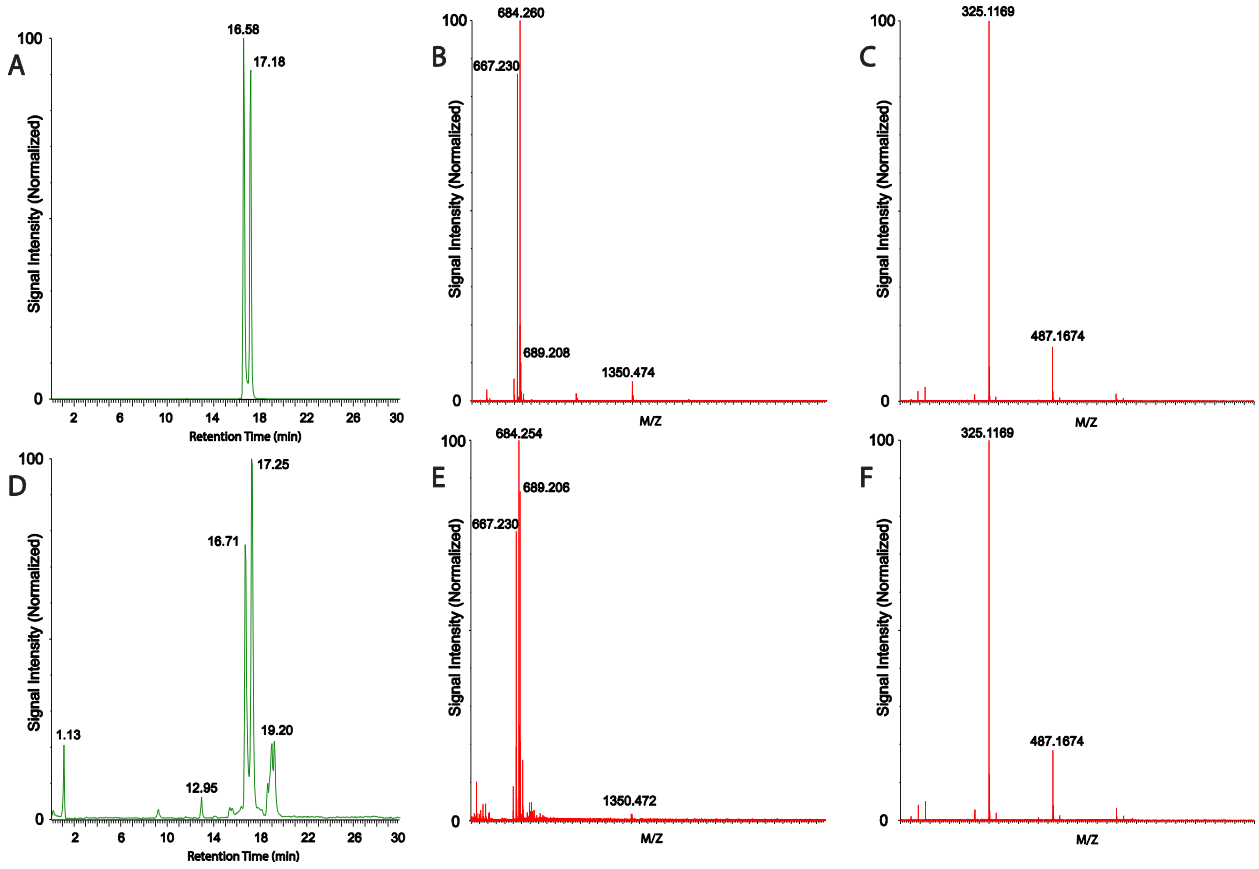

Figure S7: Identification of the MLGO produced by the action of VvEG16(ΔV152) on bMLG (Glc_4-MLGO) by LC-MS. A-C) Extracted ion chromatogram (m/z = 684.0-684.5), MS and CID MSMS spectra of The Glc_4-MLGO peak eluting at 17.2 minutes, respectively. D-F) Extracted ion chromatogram (m/z = 684.0-684.5), MS and CID MS/MS spectra of commercial G3GGG, respectively.

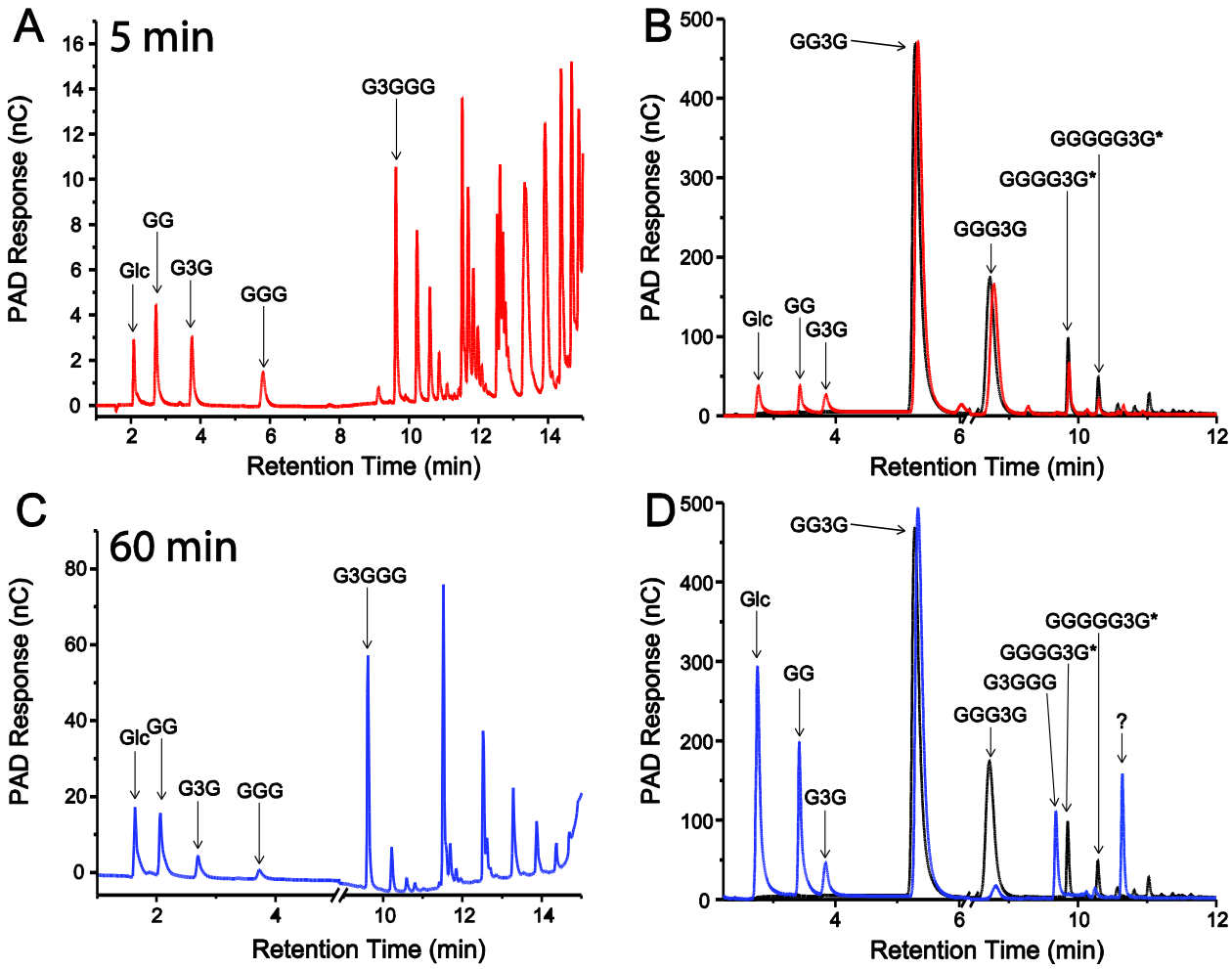

Figure S8: Time-dependent MLG hydrolysis by VvEG16(ΔV152). A) HPAEC-PAD chromatogram of the early products of MLG hydrolysis by VvEG16. B) HPAEC-PAD chromatogram of the licheninase digestion of the MLG shown in A). Licheninase-digested native MLG is shown in black and licheninase-digested VvEG16-digested MLG is shown in red. C) HPAEC-PAD chromatogram of the gel-forming MLG produced by VvEG16 digestion. D) HPAEC-PAD chromatogram of the licheninase digestion of the MLG showed in C). Licheninase-digested native MLG is shown in black and licheninase-digested VvEG16-digested MLG is shown in blue.

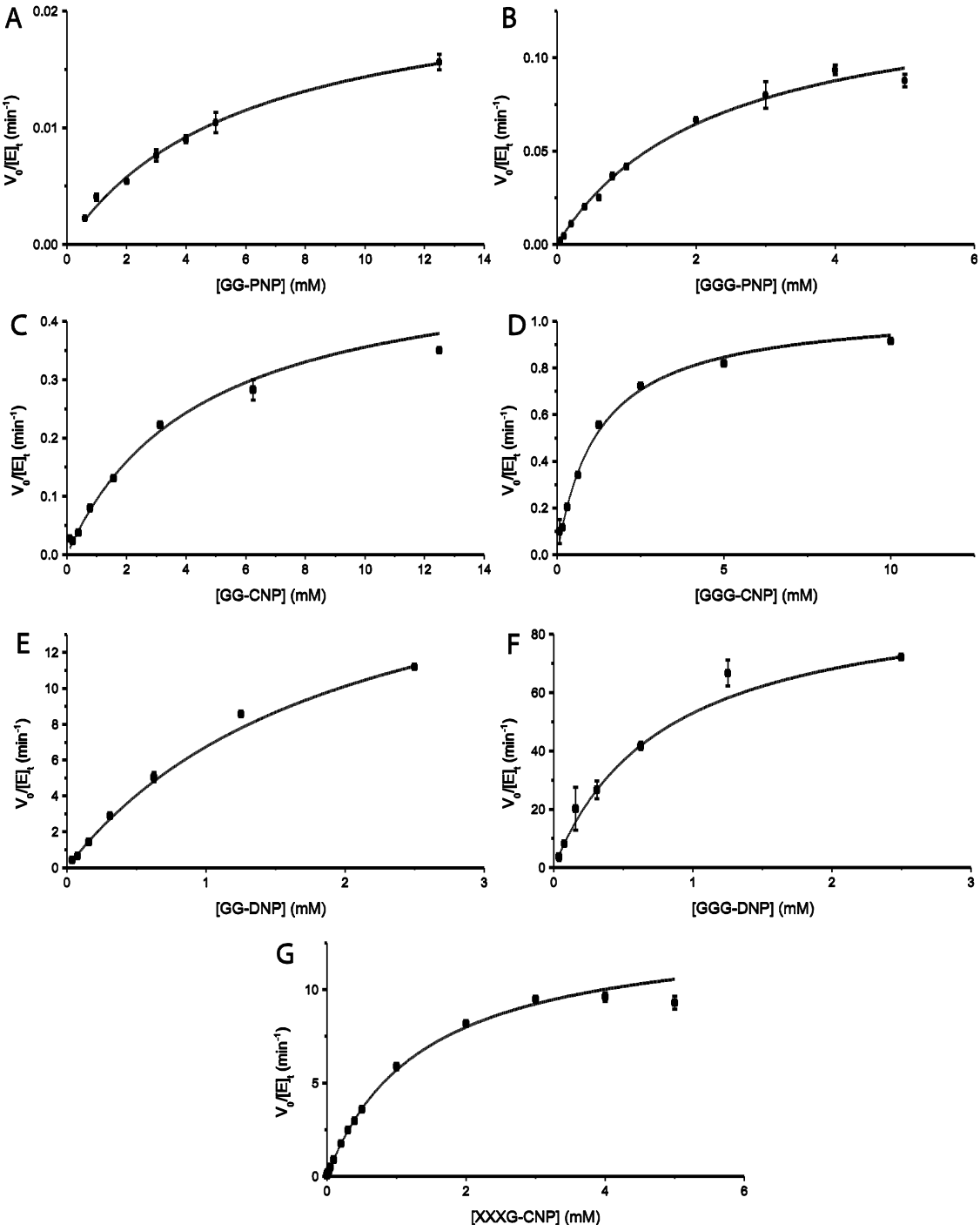

Figure S9: Kinetic data and Michaelis-Menten curves used to determine the k_{cat} and K_M values for the hydrolysis of various chromogenic substrates by VvEG16(ΔV152). Error bars are shown as the standard deviation of three technical replicates.

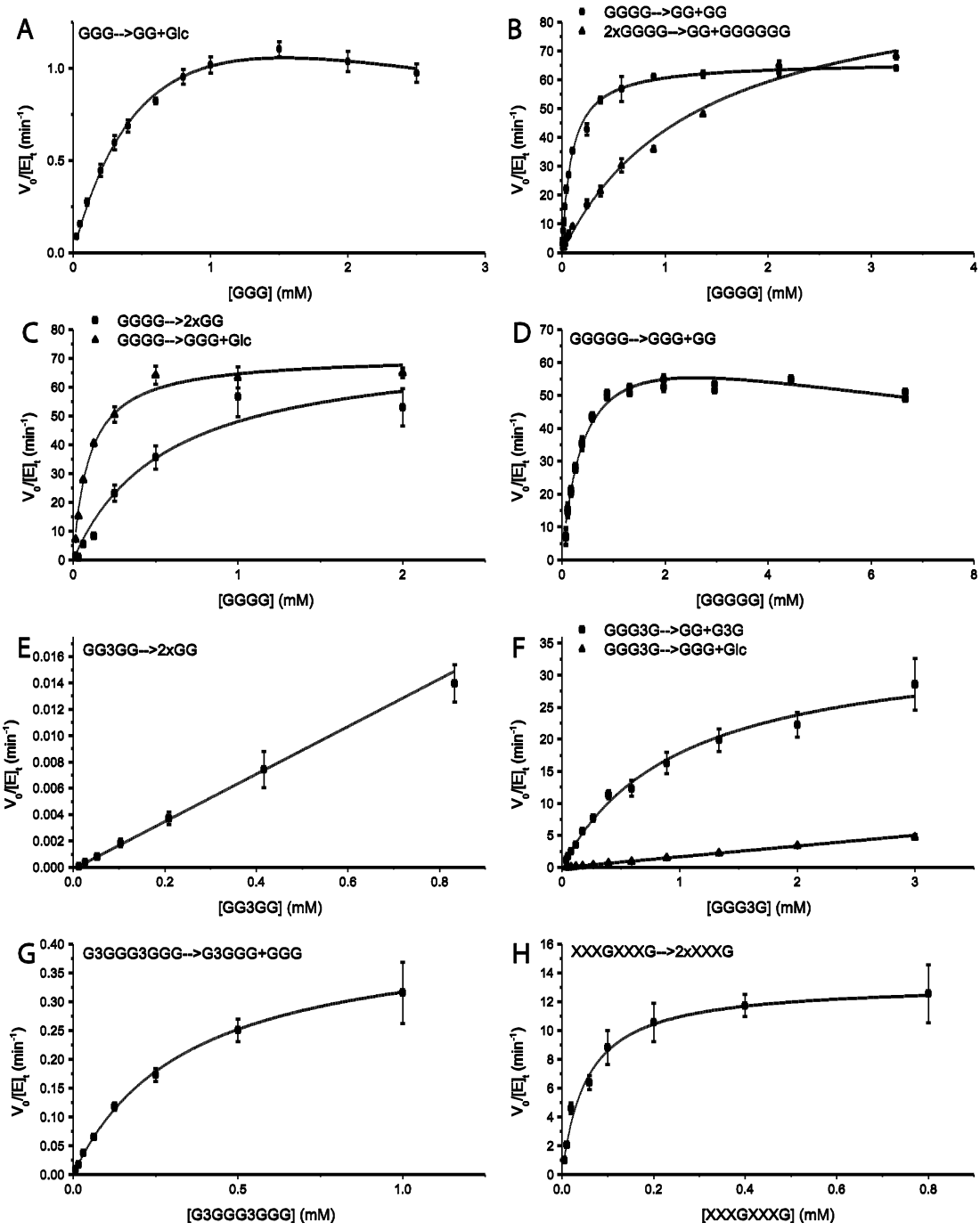

Figure S10: Kinetic data and Michaelis-Menten curves used to determine the k_{cat} and K_M values for the hydrolysis of various oligosaccharide substrates by VvEG16(ΔV152). Error bars are shown as the standard deviation of three technical replicates.

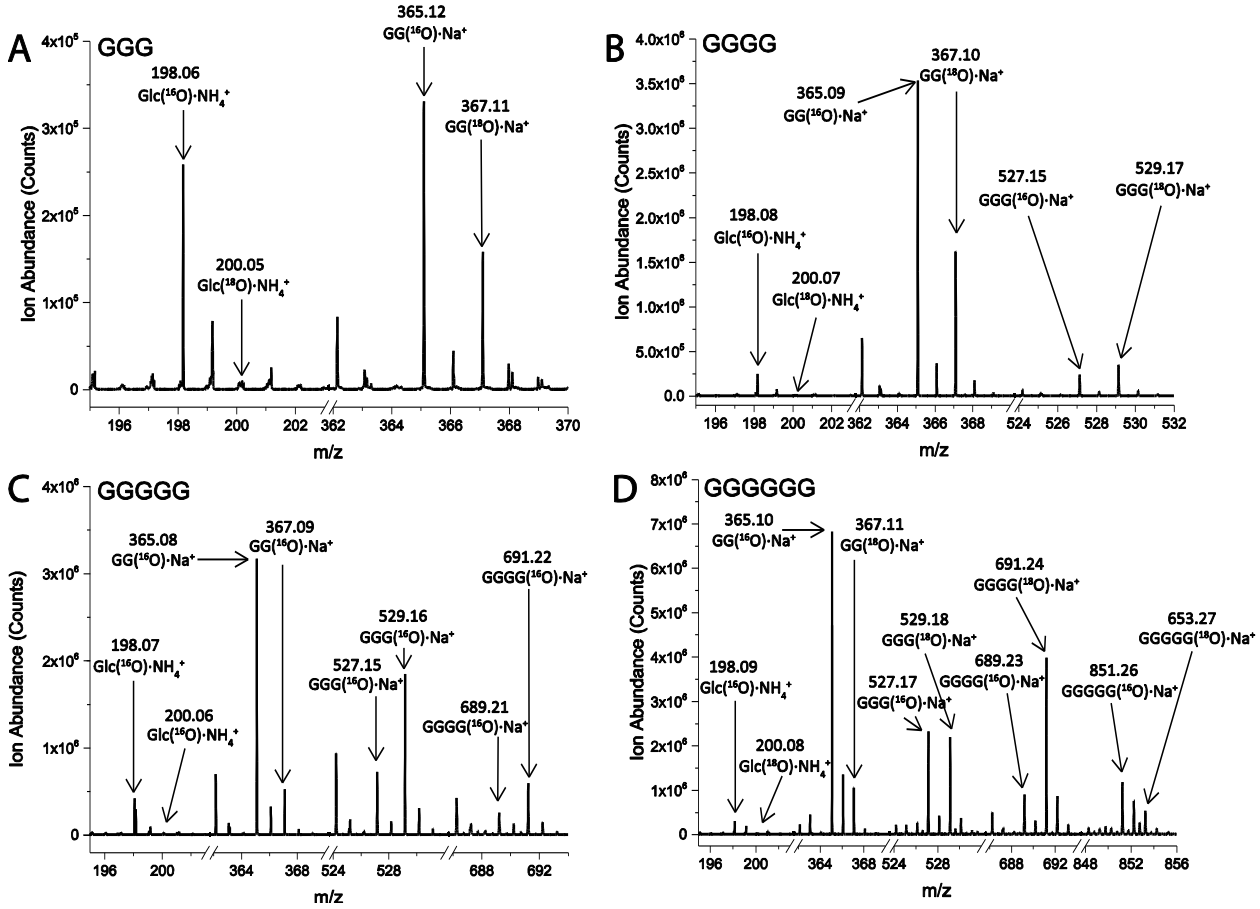

Figure S11: Mass spectra of products produced by the hydrolysis of cello-oligosaccharides by VvEG16(ΔV152) in $H_2{}^{18}O$. A) cellotriose, B) cellotetraose, C) cellopentaose, D) cellohexaose. Peak integration data can be found in table S3.

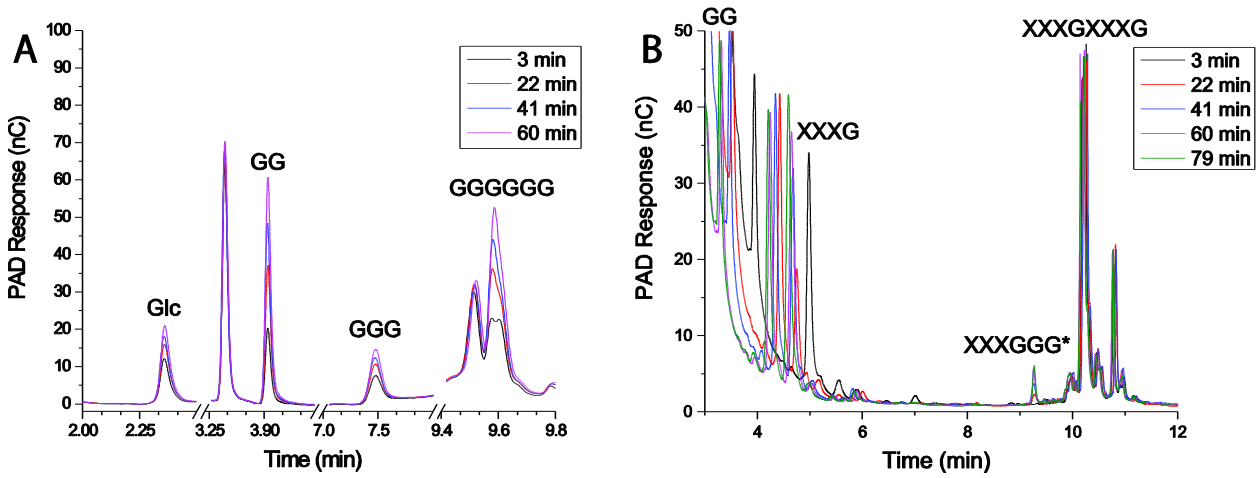

Figure S12: Homo- and hetero-transglycosylation of oligosaccharides by VvEG16(ΔV152). A) The HPAEC-PAD chromatogram of the action of VvEG16(ΔV152) on 1 mM cellotetraose over time. The increase of the peak at 9.6 minutes is indicative of the formation of cellohexaose. B) The HPAEC-PAD chromatogram of VvEG16(ΔV152) acting on 100 μM XXXGXXXG in the presence of 5 mM cellobiose over time. A small peak is observed forming at a retention time of 9.3 minutes and, later, being hydrolyzed. Though not isolated, this peak is putatively assigned as XXXGGG.

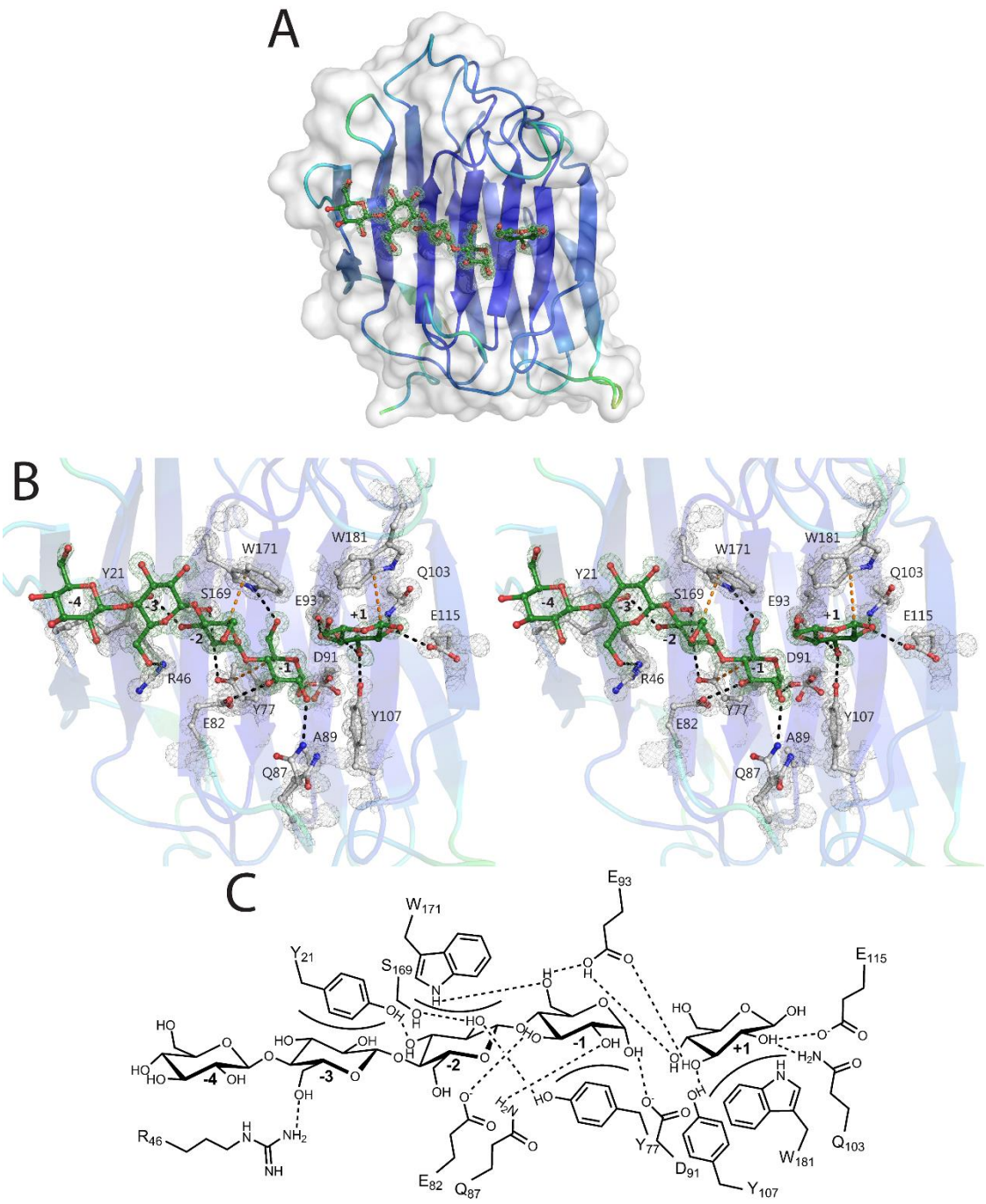

Figure S13: Structure of VvEG16(ΔV152,E89A) in complex with cellooligosaccharides. A) The asymmetric unit of this complex contains one protein molecule, shown as both a white surface representation and a cartoon representation coloured according to B-factors. The protein molecule bound to a molecule modelled as GGGG in the negative subsites and glucose in the positive subsites (both shown in green). B) and C) show the interactions between VvEG16(ΔV152,E89A) and cellooligosaccharides as in figure 3 B) and C).

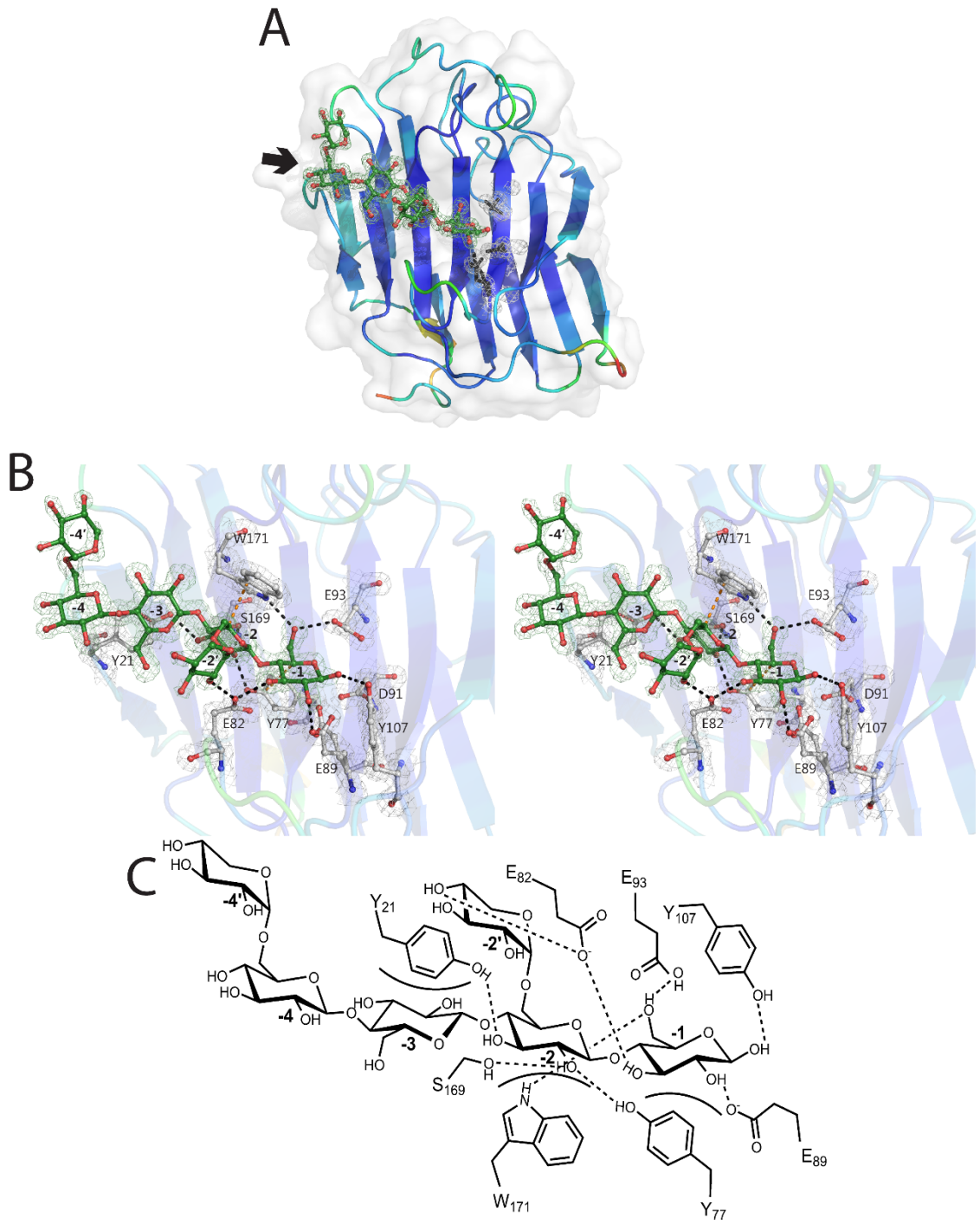

Figure S14: Structure of VvEG16(ΔV152,C22S,C188S) in complex with a xyloglucan oligosaccharide. A) The asymmetric unit of this complex contains one protein molecule, shown as both a white surface representation and a cartoon representation coloured according to B-factors. The protein molecule bound to a molecule modelled as XGXG in the negative subsites (shown in green). The location of the C22S mutation is noted with an arrow; the C188S mutation is located on the back of the enzyme from this perspective. B) and C) show the interactions between VvEG16(ΔV152, C22S,C188S) and XGXG as in figure 5 B) and C).

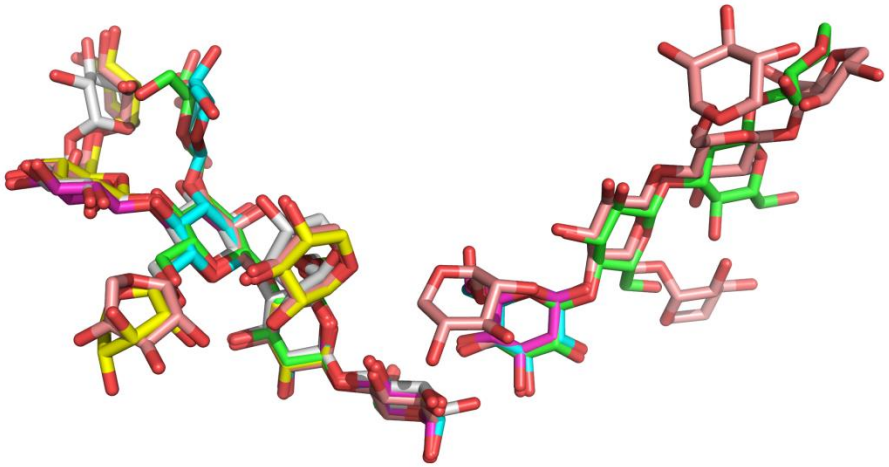

Figure S15: Superimposition of the carbohydrate ligands bound within the active site of each experimentally determined structure of VvEG16. Carbohydrates from all six chains (PDB IDs 5DZE (Magenta), 5DZF-A (Green), 5DZF-B (Cyan), 5DZG-A (Yellow), 5DZF-B (Salmon), and 5SV8 (White)) are shown.